Figure S1

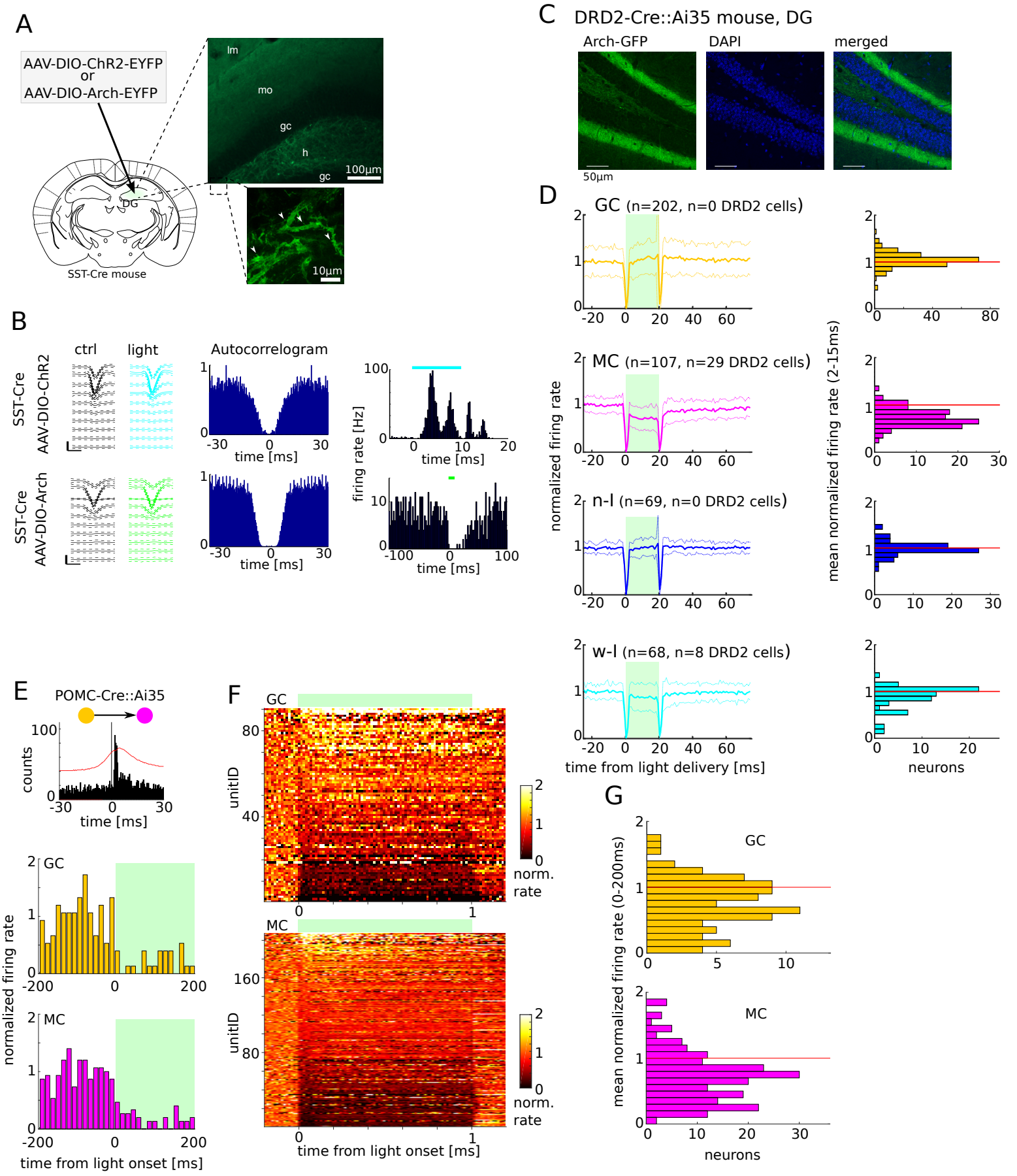
A
AAV-DIO-ChR2-EYFP
or
AAV-DIO-Arch-EYFP
lm
mo
gc
h
gc
100µm
DG
SST-Cre mouse
10µm
B
ctrl
light
SST-Cre
AAV-DIO-ChR2
SST-Cre
AAV-DIO-Arch
Autocorrelogram
time [ms]
firing rate [Hz]
time [ms]
C
DRD2-Cre::Ai35 mouse, DG
Arch-GFP
DAPI
merged
50µm
D
GC (n=202, n=0 DRD2 cells)
MC (n=107, n=29 DRD2 cells)
n-l (n=69, n=0 DRD2 cells)
w-l (n=68, n=8 DRD2 cells)
normalized firing rate
time from light delivery [ms]
mean normalized firing rate (2-15ms)
neurons
E
POMC-Cre::Ai35
counts
time [ms]
GC
MC
normalized firing rate
time from light onset [ms]
F
GC
MC
unitID
norm. rate
time from light onset [ms]
G
GC
MC
mean normalized firing rate (0-200ms)
neurons

Figure S1: Optogenetic identification of neurons, related to Figure 1

(A) AAV-DIO ChR2-EYFP or AAV-DIO-ChR2-EYFP were injected into the dentate gyrus of SST-Cre mice for optogenetic tagging of somatostatin containing (SST) interneurons. Top right: low magnification confocal image of dentate gyrus (lm, stratum lacunosum-moleculare; mo, molecular layer; gc, granule cell layer; h, hilus). Bottom: higher magnification confocal image. White arrows indicate drumstick-like spines of dendrites, characteristic of SST cells.

(B) Top: SST cell's response to blue light pulse in SST-Cre mouse injected with AAV-DIO-ChR2. A minority of SST neurons responded with rhythmic bursts at 150-250 Hz. Bottom: SST cell's response to green light pulse in SST-Cre mouse injected with AAV-DIO-Arch. Left panels: Note similar waveforms of spikes during spontaneous activity (control, ctrl) and during light stimulation (light).

(C) Histological section of the dentate gyrus in a DRD2-Cre::Ai35 mouse

(D) Population response shown for each neuron type in DRD2-Cre::Ai35 mice ($n = 4$). MC population activity significantly decreased ($P < 0.00001$, Wilcoxon signed rank test) while GC population activity significantly increased ($P < 0.00001$, Wilcoxon signed rank test), indicating an overall strong feed-forward inhibitory control of mossy cells on granule cell activity (via assumed intercalated inhibitory interneurons).

(E) Activity patterns in POMC-Cre::Ai35 mice. Green light induced suppression of spiking in both GC and MC. Top: short time scale cross-correlogram in a pair of monosynaptically connected GC-MC pair. The strong disfacilitation of MC by GC may be responsible for the secondary decrease of MC activity.

(F,G) 1sec green light delivery modified the activity of both GC and MC in POMC-Cre::Ai35 mice ($n = 2$). While a similar fraction of GC and MC decreased their activity (bottom part of the panel), a small minority increased their spiking (top), likely due to disinhibition. Due to such circuit effects, reliable optogenetic identification of GC is not feasible.

Figure S2

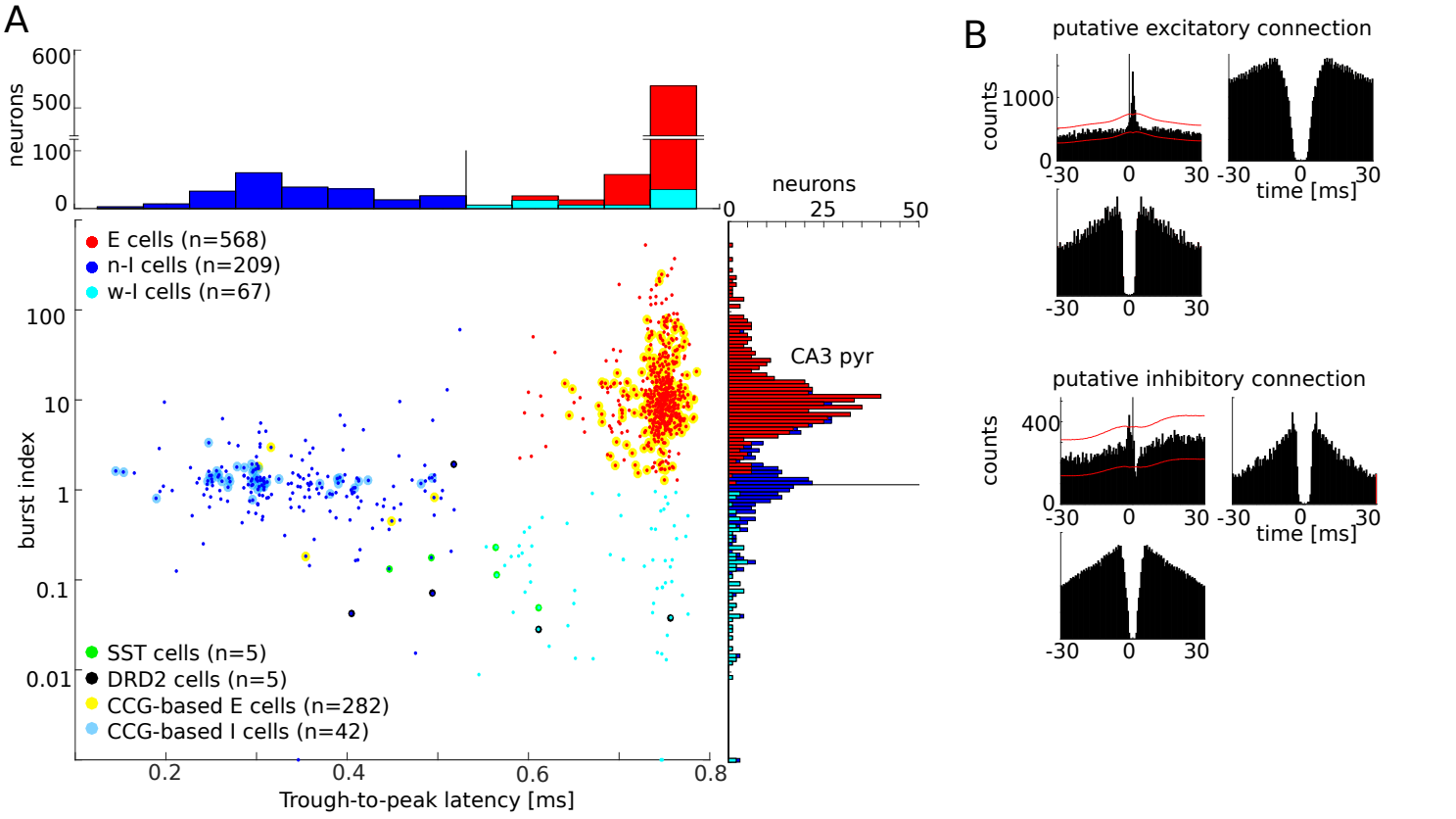


Figure S2: Classification of CA3 units, related to Figure 1
(A) Units in the CA3 region (n = 777 from n = 6 mice) were first classified based on trough-to-peak latency and burst index as in Figure 1a, assisted by physiological interactions. Other abbreviations are as in Figure 1. (B) Top: an example of putative excitatory monosynaptic connection between two neurons. Autocorrelograms of the partner cells and cross-correlogram showing sharp peak < 2ms after the reference spike. Bottom: an example of putative inhibitory monosynaptic connection. Note significant dip of spiking of the postsynaptic neurons in the 1-3 ms bins after the spike of the putative inhibitory interneuron (time zero).

Figure S3

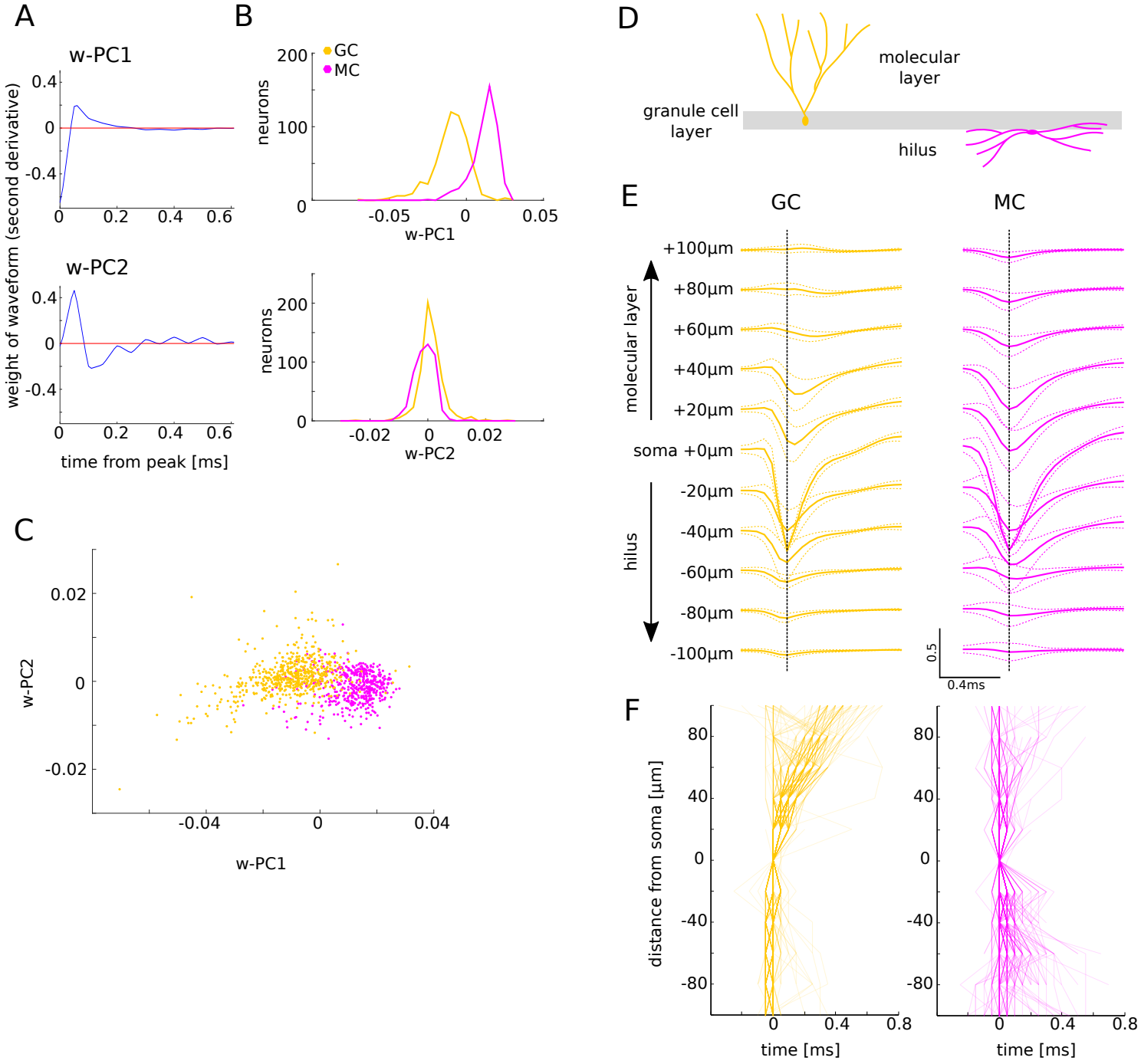


Figure S3: Waveform classification and depth profile of GC and MC spikes, related to Figure 1
(A) w-PC1 (Top) and w-PC2 (bottom) as a result of waveform PCA.
(B) w-PC1 (Top) and w-PC2 (bottom) amplitude distribution for GC and MC.
(C) GC and MC are displayed as a function of w-PC1 and w-PC2. Note that w-PC1 strongly differentiated between the two excitatory cell groups but w-PC2 also contributed.
(D) Schema of the anatomical location and dendritic arbors of GC and MC.
(E) Unit waveforms (mean ± s.d.) of all GC and MC at different vertical distances from the soma.
(F) Trough latency curves as a function of distance from the soma of GC and MC. Since recordings were made parallel with the somatodendritic axis of GC, the backpropagating action potentials with characteristic delays could be also detected in the extracellular unit recordings. In contrast, MC dendrites run perpendicular to the recording sites, thus no such delays are present.

Figure S4

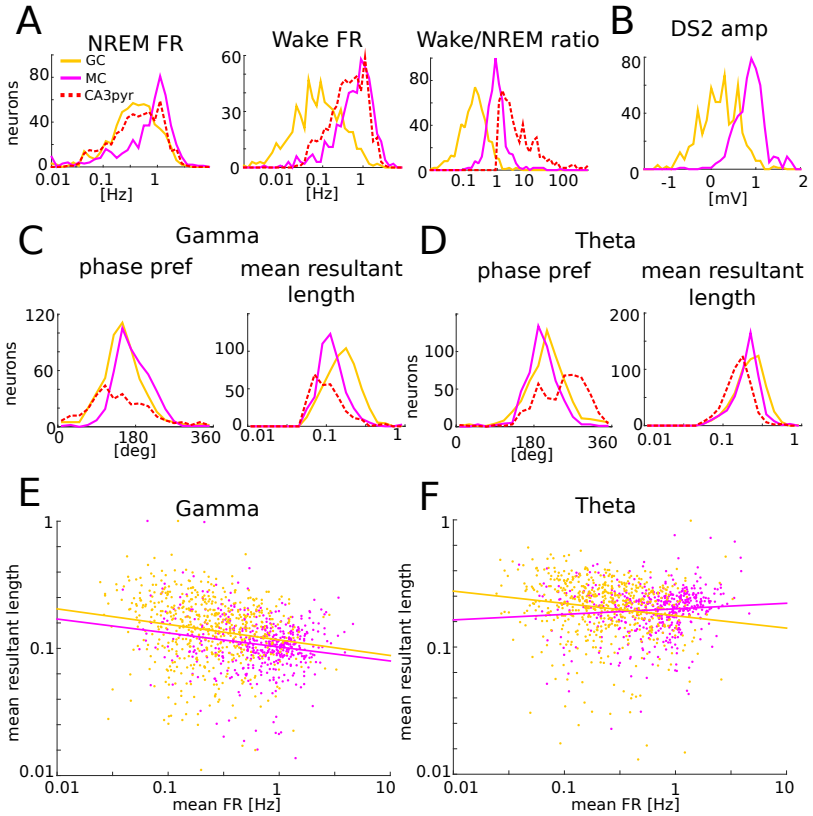


Figure S4: Physiological properties of identified GC, MC, and CA3 pyramidal cells, related to Figure 2
(A) Log firing rates of GC (yellow), MC (magenta), CA3pyr (red) during nonREM sleep (NREM FR), waking, and the ratio of NREM to wake firing rates. Note very slow firing rates of GC.
(B) DS2 amplitude distribution for GC and MC. Average dentate spike amplitude was measured at the recording site of the largest amplitude of a given unit. Note that the majority of MC recording sites were associated with positive DS2, i.e., they were located below the middle of the granule cell layer. GC, on the other hand were associated with both positive and negative DS2, i.e., largely corresponding to the granule cell layer.
(C) Phase preference of individual units (left) and the mean resultant length (right) for gamma oscillations.
(D) Phase preference of individual units (left) and the mean resultant length (right) for theta oscillations.
(E) Log(mean resultant length for gamma oscillation) and log(mean FR) were negatively correlated for both GC (yellow, $R = -0.18$, $P < 0.0001$) and MC (magenta, $R = -0.18$, $P < 0.0001$). Dotted line: linear regression fit.
(F) Log (mean resultant length for theta oscillation) and log(mean FR) were negatively correlated for GC ($R = -0.16$, $P = 0.00012$) but not for MC ($R = 0.09$, $P = 0.046$). Dotted line: liner regression fit.

Figure S5

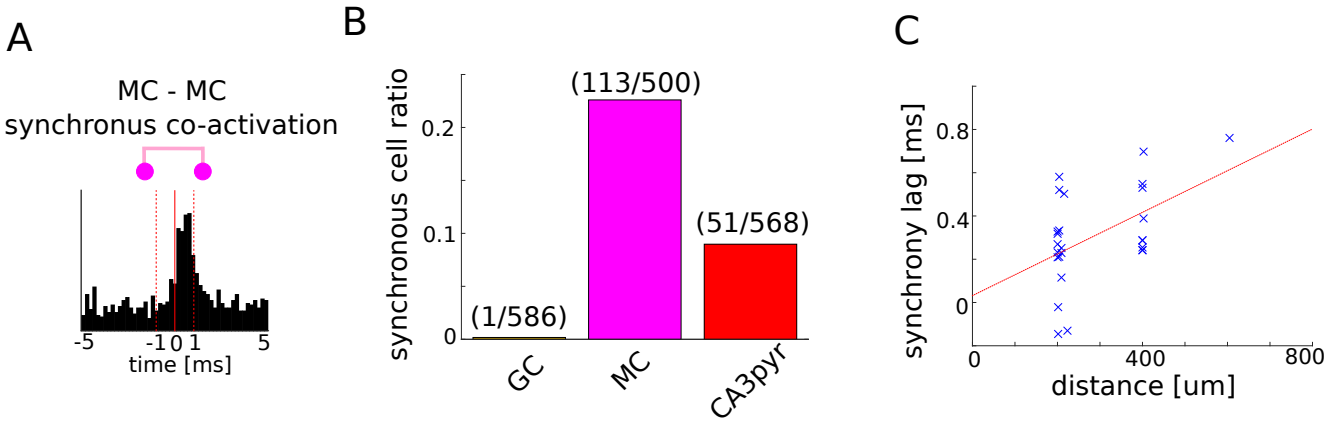


Figure S5: Synchronous (< 1ms; "zero time lag"; Diba et al., 2014) co-activation of neurons in DG and CA3, related to Figure 3

(A) Example of sub-millisecond synchronous co-activation.

(B) Fractions of synchronous unit co-activations of GC, MC, and CA3pyr.

(C) Time lag as a function of medio-lateral distance of the recorded CA3-CA3 pyramidal neuron pairs ($R = 0.50$, $P < 0.001$).

Figure S6

A


B

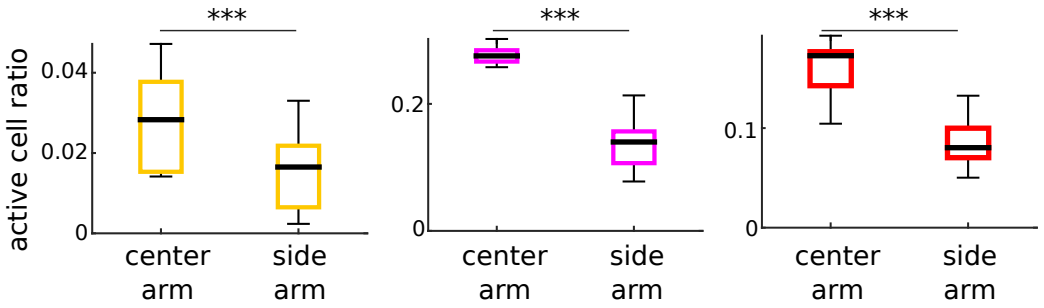


C

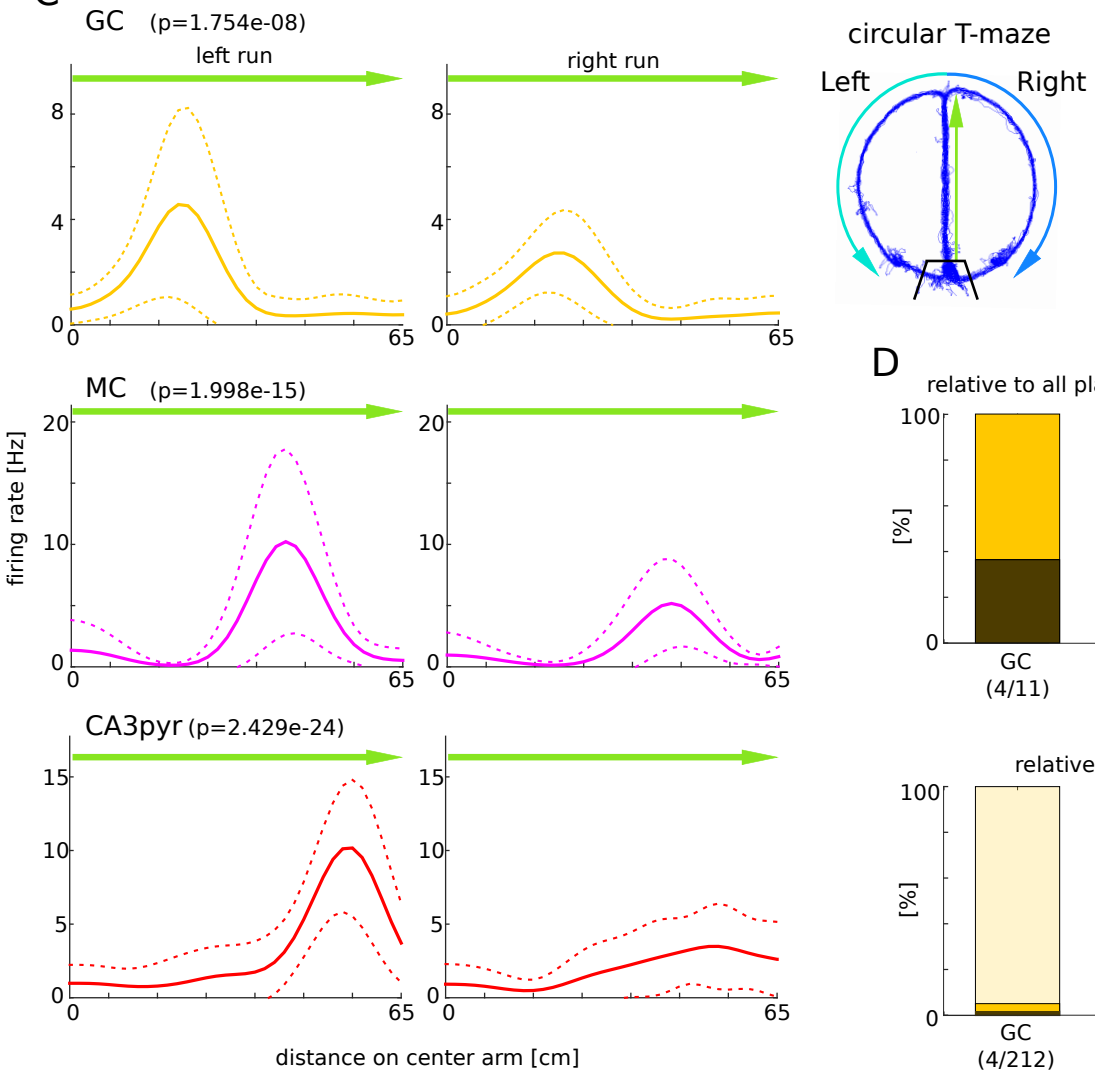


D

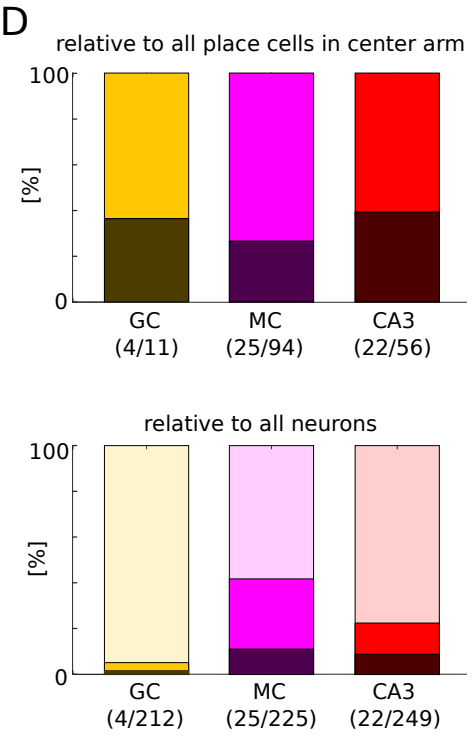

Figure S6: Details of the open field and the circular T-mazes, related to Figure 5 and 6
(A) Photographs of maze A and maze B. Note differences of color and texture of the sides and floor between the two mazes.
(B) Ratio of the fraction of active units in the center and side arms for GC (left), MC (middle), and CA3pyr neurons (right).
(C) Example 'splitter' cells from the GC, MC, CA3pyr groups. Rate maps in the center arm during left run and right run are presented (mean ± s.d.) separately. Top right: schema of the circular T-maze.
(D) Top: Relative ratio of splitter cells to all place cells in the center arm. Black bar graph shows the percentage of splitter cells. Bottom: ratio of splitter cells to all neurons for each neuron type. Pale color bar graph represents neurons without place field.

# Figure S7

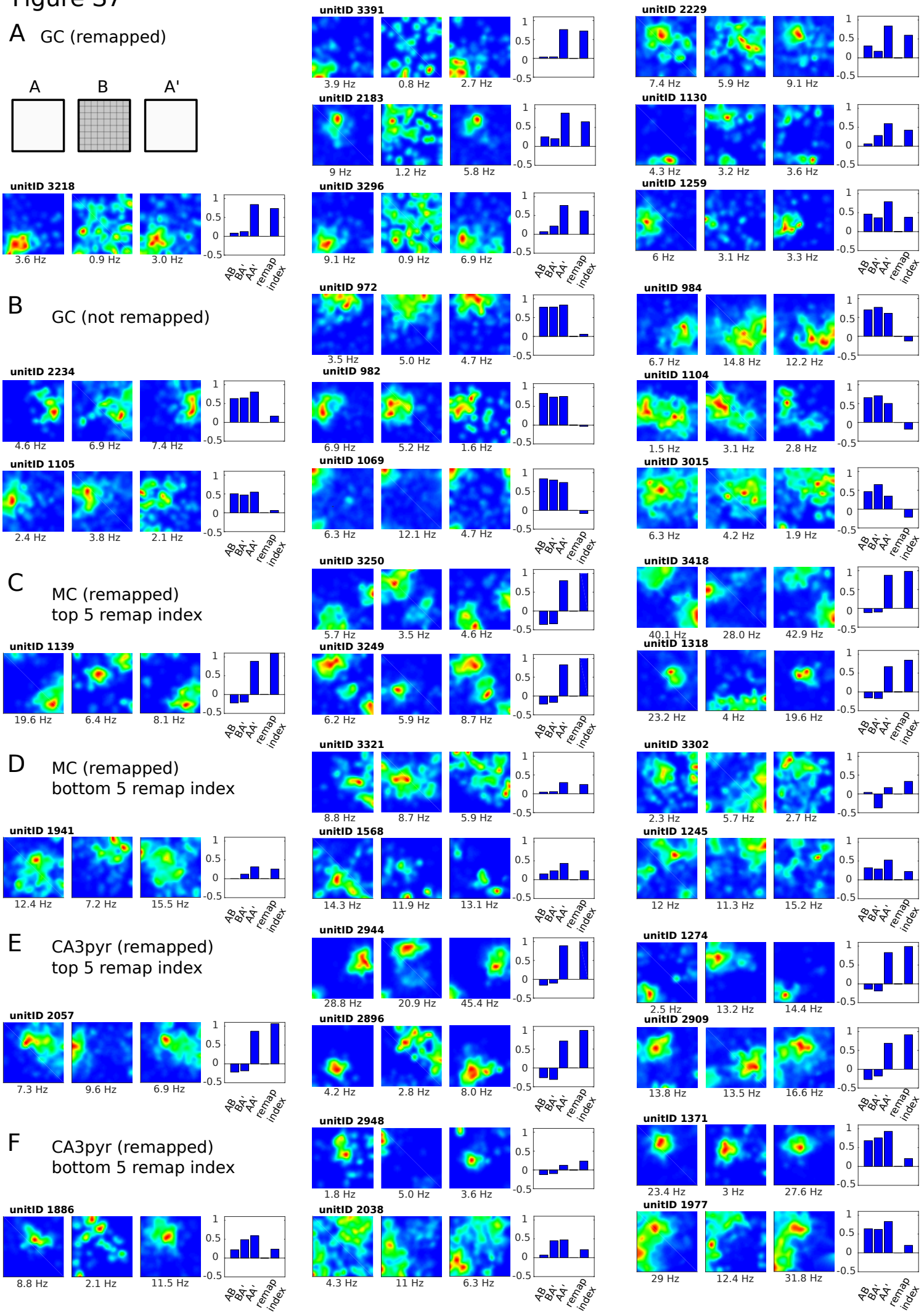
A
GC (remapped)
A
B
A'
unitID 3218
3.6 Hz
0.9 Hz
3.0 Hz
B
GC (not remapped)
unitID 2234
4.6 Hz
6.9 Hz
7.4 Hz
unitID 1105
2.4 Hz
3.8 Hz
2.1 Hz
C
MC (remapped)
top 5 remap index
unitID 1139
19.6 Hz
6.4 Hz
8.1 Hz
D
MC (remapped)
bottom 5 remap index
unitID 1941
12.4 Hz
7.2 Hz
15.5 Hz
E
CA3pyr (remapped)
top 5 remap index
unitID 2057
7.3 Hz
9.6 Hz
6.9 Hz
F
CA3pyr (remapped)
bottom 5 remap index
unitID 1886
8.8 Hz
2.1 Hz
11.5 Hz
unitID 3391
3.9 Hz
0.8 Hz
2.7 Hz
unitID 2183
9 Hz
1.2 Hz
5.8 Hz
unitID 3296
9.1 Hz
0.9 Hz
6.9 Hz
unitID 972
3.5 Hz
5.0 Hz
4.7 Hz
unitID 982
6.9 Hz
5.2 Hz
1.6 Hz
unitID 1069
6.3 Hz
12.1 Hz
4.7 Hz
unitID 3250
5.7 Hz
3.5 Hz
4.6 Hz
unitID 3249
6.2 Hz
5.9 Hz
8.7 Hz
unitID 3321
8.8 Hz
8.7 Hz
5.9 Hz
unitID 1568
14.3 Hz
11.9 Hz
13.1 Hz
unitID 2944
28.8 Hz
20.9 Hz
45.4 Hz
unitID 2896
4.2 Hz
2.8 Hz
8.0 Hz
unitID 2948
1.8 Hz
5.0 Hz
3.6 Hz
unitID 2038
4.3 Hz
11 Hz
6.3 Hz
unitID 2229
7.4 Hz
5.9 Hz
9.1 Hz
unitID 1130
4.3 Hz
3.2 Hz
3.6 Hz
unitID 1259
6 Hz
3.1 Hz
3.3 Hz
unitID 984
6.7 Hz
14.8 Hz
12.2 Hz
unitID 1104
1.5 Hz
3.1 Hz
2.8 Hz
unitID 3015
6.3 Hz
4.2 Hz
1.9 Hz
unitID 3418
40.1 Hz
28.0 Hz
42.9 Hz
unitID 1318
23.2 Hz
4 Hz
19.6 Hz
unitID 3302
2.3 Hz
5.7 Hz
2.7 Hz
unitID 1245
12 Hz
11.3 Hz
15.2 Hz
unitID 1274
2.5 Hz
13.2 Hz
14.4 Hz
unitID 2909
13.8 Hz
13.5 Hz
16.6 Hz
unitID 1371
23.4 Hz
3 Hz
27.6 Hz
unitID 1977
29 Hz
12.4 Hz
31.8 Hz
1
0.5
0
-0.5
AB
BA'
AA'
remap
index

Figure S7: Examples of place field remapping of GC, MC, and CA3 pyramidal cells, related to Figure 6
(A) Rate maps of representative GCs which showed significant place field remapping across open fields (remap index >0.2).
(B) Rate maps of GCs without significant remapping (remap index < 0.2). The majority of granule cells did not show significant remapping (Figure 6).
(B) Rate maps of MCs with the largest five remap indexes (remap index >0.2).
(C) Rate maps of MCs with the smallest five remap indexes (remap index >0.2).
(D) Rate maps of CA3 pyramidal cells with the largest five remap indexes (remap index >0.2).
(E) Rate maps of CA3 pyramidal cells with the smallest five remap indexes (remap index >0.2). Note dominant global remapping of most MC and CA3 pyramidal cells.

# Table S1

| Mouse ID | Mouse genotype (+ virus type) | Probe type[1] | Probe orient[2] | Probe position [AP, ML][3] | | | BW [g] | Age [mo] | Ses[4] | Task[5] | | DG unit | | | CA3 | DRD2 cell | | SST cell | |
|---|---|---|---|---|---|---|---|---|---|---|---|---|---|---|---|---|---|---|---|
| | | | | center | medial edge | lateral edge | | | | T | OF | All | GC | MC | All | DG | CA3 | DG | CA3 |
| YM20 | SST-Cre + AAV-DIO-ChR2 | 6shank | L | [-1.9, -1.2] | [-1.6, -0.9] | [-2.3, -1.6] | 33 | 5 | 5 | | | 58 | 4 | 25 | | | | 4 | |
| YM21 | SST-Cre + AAV-DIO-ChR2 | Linear | -- | [-1.9, -1.2] | | | 27 | 6 | 1 | | | | | | | | | | |
| YM23 | SST-Cre + AAV-DIO-Arch | 6shank | L | [-1.9, -1.2] | [-1.6, -0.9] | [-2.3, -1.6] | 33 | 6 | 3 | | | 59 | 28 | 11 | | | | 2 | |
| YM33 | POMC-Cre::Ai35 | 8shank | L | [-1.9, -1.2] | [-1.4, -0.7] | [-2.4, -1,7] | 36 | 6 | 9 | x | | 236 | 37 | 72 | | | | | |
| YM37 | SST-Cre + AAV-DIO-ChR2 | 6shank | L | [-1.9, -1.2] | [-1.6, -0.9] | [-2.3, -1.6] | 30 | 11 | 5 | x | | 42 | 22 | 9 | | | | 0 | |
| YM38 | SST-Cre + AAV-DIO-ChR2 | 6shank | L | [-1.9, -1.2] | [-1.6, -0.9] | [-2.3, -1.6] | 30 | 10 | 1 | x | | 18 | 6 | 4 | | | | 1 | |
| YM39 | SST-Cre + AAV-DIO-ChR2 | 8shank | T | [-1.9, -1.2] | [-2.4, -0.7] | [-1.4, -1.7] | 32 | 11 | 7 | x | | 105 | 41 | 29 | 57 | | | 3 | 5 |
| YM40 | SST-Cre + AAV-DIO-ChR2 | 8shank | T | [-1.9, -1.2] | [-2.4, -0.7] | [-1.4, -1.7] | 40 | 8 | 3 | x | | 30 | 23 | 0 | | | | | |
| YM41 | WT | 8shank | T | [-1.9, -1.6] | [-2.4, -1.1] | [-1.4, -2.1] | 43 | 10 | 10 | x | x | 292 | 134 | 82 | 158 | | | | |
| YM42 | POMC-Cre::Ai35 | 8shank | T | [-1.9, -1.6] | [-2.4, -1.1] | [-1.4, -2.1] | 37 | 11 | 15 | x | x | 272 | 67 | 144 | 298 | | | | |
| YM44 | POMC-Cre::Ai35 | 6shank | T | [-1.9, -1.6] | [-2.4, -1.1] | [-1.7, -1.8] | 44 | 11 | 3 | x | x | 18 | 8 | 1 | | | | | |
| YM45 | Drd2-Cre::Ai35 | 8shank | T | [-1.9, -1.6] | [-2.4, -1.1] | [-1.4, -2.1] | 37 | 8 | 5 | x | x | 37 | 24 | 7 | | | | | |
| YM51 | Drd2-Cre::Ai35 | 6shank | L | [-1.9, -1.2] | [-1.6, -0.9] | [-2.3, -1.6] | 29 | 4 | 4 | | | 51 | 32 | 3 | | 1 | 0 | | |
| YM54 | Drd2-Cre::Ai35 | 8shank | T | [-1.9, -1.6] | [-2.4, -1.1] | [-1.4, -2.1] | 27 | 5 | 5 | | | 131 | 46 | 54 | 103 | 21 | 3 | | |
| YM55 | Drd2-Cre::Ai35 | 8shank | T | [-1.9, -1.6] | [-2.4, -1.1] | [-1.4, -2.1] | 25 | 4 | 9 | | x | 71 | 37 | 6 | 139 | 8 | 2 | | |
| YM56 | Drd2-Cre::Ai35 | 8shank | T | [-1.9, -1.6] | [-2.4, -1.1] | [-1.4, -2.1] | 24 | 4 | 9 | | x | 187 | 88 | 42 | 90 | 7 | 0 | | |

1. Probe type; 6shank: Buzsaki64sp (10 sites per shank), 8shank: Buzsaki64 (8 sites per shank), Linea: 32 site linear probe.
2. Probe orient (orientation); L: parallel to longitudinal axis, T: parallel to transverse axis.
3. anteroposterior (AP) and mediolateral (ML) distance from bregma [mm].
4. Ses: number of sessions for each mouse.
5. Task; T: circular T-maze, OF: open field environments (A, B).

Table S1: List of mice, related to Figure 1